RSC Applied Polymers

ROYAL SOCIETY OF CHEMISTRY

PAPER

View Article Online
View Journal | View Issue

Cite this: *RSC Appl. Polym.*, 2024, **2**, 857

Polymer macroligands passivate halide perovskite surfaces†

Mykyta Dementyev, [a] Lindsay F. Jones, [a] Michael C. Brennan, [c,d] Tod A. Grusenmeyer, [c] Seth D. Waugaman, [e] Robert T. Mathers [e] and Robert J. Hickey *[a,b]

Hybrid organic–inorganic hybrid perovskite (OIP) nanocrystals have gained considerable excitement due to high photoluminescence (PL) quantum yields, bandgap tunability, and narrow band emission, which are essential for photovoltaic devices, light emitting diodes (LEDs), and optical displays. While researchers have designed numerous ways to synthesize OIP nanomaterials, there is still a need to explore faster, cheaper, and scalable methods of making stable, highly performing nanomaterials for device applications. Polymers are commonly used to encapsulate OIP nanomaterials, yielding enhancements in long-term stability as well as improved PL properties. However, the exact impact of polymer chemical composition on perovskite nanocrystal growth and material properties is still unknown. Here, we reveal how polymer chemical composition directly modulates the formation of perovskite composite materials with ~75 wt% perovskite with respect to polymer and the optical properties during a one-step, co-precipitation synthesis procedure. Specifically, a series of polymers were explored, poly(styrene) (PS), poly(4-vinylpyridine) (P4VP), poly(ethyleneimine) (PEI), poly(ethylene oxide) (PEO), poly(vinylpyrrolidone) (PVP), and poly (methyl methacrylate) (PMMA), to compare the structure and optical properties of the resulting OIP materials. Polymers with nitrogen-containing functional groups, such as amides, pyridine, and amines, are shown to preferentially bind to and passivate perovskite surfaces, acting as polymer macroligands. Nitrogen atoms in the polymer coordinate with under-coordinated lead ions on the perovskite surface, passivating surface defects and leading to an enhancement in the optical properties. Polymer macroligands also promote nanocrystal formation in a similar method as prototypical surface-active ligands used in nanocrystal syntheses. This work uncovers design rules for creating composite materials exhibiting desired nanostructures and enhanced optical properties for future OIP devices through the use of polymer macroligands.

Received 27th March 2024,
Accepted 21st June 2024

DOI: 10.1039/d4lp00114a

rsc.li/rscapplpolym

Introduction

Hybrid organic/inorganic halide perovskites with ABX_3 stoichiometry (A = $CH_3NH_3^+$, $CH(NH_2)_2^+$, Cs^+, B = Pb^{2+} or Sn^{2+}, and X = Cl^-, Br^- or I^-) are attractive alternatives to replace current semiconductor materials for applications in photovoltaics,[1–4] solar water splitting,[5] photodetectors,[6,7] imaging,[8] light emitting diodes (LEDs),[9–11] and optical displays[12,13] due to enhanced device performance and unique optical properties. Such optical properties are a result of long-range electron and hole transport,[14] impressive absorption coefficients over a large wavelength range (*e.g.*, 380–750 nm),[15] and excellent photoluminescence (PL) quantum yields (QY).[16] Thus, enabling the material to be highly suitable for optoelectronic and photovoltaic applications. Additionally, the low cost of material synthesis makes perovskite materials a viable candidate to replace current semiconductor materials.[17] Hot-injection synthetic approaches as well as ligand assisted reprecipitation techniques are the most common and straightforward methods to prepare ABX_3 perovskite nanomaterials.[9,13,18] Even though perovskite materials with a wide range of domain sizes show great potential for optic and electronic applications, low stability towards moisture, UV-Vis irradiation, and heat limit their practical use in devices.

[a]*Materials Science and Engineering, The Pennsylvania State University, University Park, PA, 16802, USA. E-mail: rjh64@psu.edu*
[b]*Materials Research Institute, The Pennsylvania State University, University Park, PA, 16802, USA*
[c]*Air Force Research Laboratory, Materials and Manufacturing Directorate, Wright-Patterson Air Force Base, Dayton, Ohio 45433, USA*
[d]*Azimuth Corporation, 2079 Presidential Dr. #200, Fairborn, OH 45342, USA*
[e]*Chemistry, The Pennsylvania State University, New Kensington, PA, 15068, USA*

† Electronic supplementary information (ESI) available: Experimental details and polymer characterization results such as SEC on synthesized PS and molecular weights with T_g on all polymers used in film preparation. See DOI: https://doi.org/10.1039/d4lp00114a

Small molecule ligands have been extensively used for controlled synthesis of perovskite nanocrystals.[13,19–21] Issues of agglomeration and reduced stability against water/air remains an issue, due to the ionic nature of perovskite crystals along with the dynamic nature of small molecule ligand binding to the perovskite surface.[22] Polymers have demonstrated to be superior to small molecule ligands in producing stable perovskite crystals while maintaining and in some cases improving optical properties. For instance, Yoon *et al.* indicated perovskite nanocrystals synthesized with star-like copolymers showed superior water stability and prevented agglomeration as compared to perovskite synthesized with oleylamine and oleic acid.[23] In another report written by Wang *et al.*, stability of the photoluminescence of synthesized perovskite material after exposing to polar and nonpolar solvents was significantly enhanced when polyzwitterionic ligands were used as compared to perovskite materials synthesized with oleylamine and oleic acid ligands.[24] Overall, polymers offer additional venues for synthesizing perovskite materials with enhanced stability and optical properties.

Post-synthetic encapsulation of ABX_3 perovskites in polymer matrices has been shown to improve long-term stability while maintaining optical properties.[25–31] A thin, passivating layer of poly(methyl methacrylate) (PMMA) was found to prevent moisture absorption and maintain the high power conversion efficiency (PCE) of fabricated solar cells.[25] Similarly, poly(styrene) (PS) was utilized as a capping layer to create an inner-encapsulated perovskite solar cell with enhanced PCE.[26] In both examples, the polymers used to create composite perovskite/polymer solar cells improve device performance by acting as an inert component for previously synthesized crystals that increase material stability. Additionally, Wang *et al.* reported a microencapsulation strategy to obtain well-dispersed organic–inorganic hybrid perovskite (OIP) nanocrystals in polymer matrices using a polymer–solvent swelling–deswelling phenomenon, where the photoluminescence efficiency of the film was consistent in boiling water for 60 days.[28] Research reported by Wei *et al.*, Xuan *et al.*, and Papagiorgis *et al.* showed that perovskite nanocrystals synthesized *via* hot injection capped with small molecule ligands oleylamine and oleic acid ligands where blended in different polymer matrixes. In these studies, post-synthetic polymer encapsulation prevented nanocrystal degradation and, in some cases, increased photoconversion efficiency.[29–31] However, the encapsulation and dispersion of perovskites in most polymers is predicated on the fact that polymers are inert components, which limits the possibilities of enhancing the optical properties of the materials through synergistic polymer/inorganic effects.

Polymers have been shown to play an active role as ligands in the synthesis of perovskite nanocrystals.[32,33] Active polymers, when present with the perovskite precursors, positively affect the final formation of the crystals.[34–38] Conversely, inert polymers typically do not contribute to the final form of the crystals because the two components are combined post-synthesis. Polymer nanoreactors have been shown to template the synthesis of perovskite nanocrystals in nanoscale colloids.[39] Furthermore, adding poly(ethylene oxide) (PEO) to a perovskite precursor solution results in the formation of composite materials with reduced point defects, leading to improved PCE without hysteresis.[35,36] In one study, improved device performance was linked to energy funneling from smaller grains to larger grains of perovskite crystals, which were formed in the presence of PEO.[35] PEO is also reported to coordinate with the perovskite surfaces, passivating the surface and leading to an increase in the charge transfer rate.[35,36] In another instance, poly(acrylonitrile) (PAN) has been used to produce high green fluorescence with photoluminescence quantum yield (PLQY) of up to 88% in both circular and non-polarized luminescence in OIP nanofibers synthesized by a fiber spinning chemistry method.[37,39] While the majority of examples in the literature use polymers as a protective coating with respect to perovskite/polymer composites, recent findings suggest benefits from involving active polymers. Polymers that display favorable interactions with the surfaces of perovskites significantly influence the resulting size, shape, and optical properties of the nanocrystals.[23,40] Even though polymers are widely used in the field, the effects of interactions of the polymer with the nanocrystal surface on perovskite nanocrystal formation and optical properties are underexplored.

Here, we reveal how polymer chemical composition influences the optical properties of methylammonium lead bromide ($CH_3NH_3PbBr_3$ or $MAPbBr_3$) halide perovskites through surface interactions during the crystal growth process. A new single-step co-precipitation synthesis method is employed to form composite perovskite/polymer materials with ~75 wt% perovskite with respect to polymer. Specifically, perovskite precursors ($PbBr_2$ and MABr) and polymer are initially dissolved together in *N*,*N*-dimethylformamide (DMF) and then injected into toluene, which acts as a coagulation bath. A series of polymers, poly(styrene) (PS), poly(4-vinylpyridine) (P4VP), poly(ethyleneimine) (PEI), poly(ethylene oxide) (PEO), poly(vinylpyrrolidone) (PVP), and poly(methyl methacrylate) (PMMA), demonstrate a variety of perovskite/polymer interactions through changes in polymer functional groups. These changes result in either bulk or nanocrystalline perovskite materials. Results indicate that OIP materials using nitrogen-containing polymers such as PEI, P4VP, and PVP exhibit pronounced PL as compared to nitrogen-absent polymers PS, PEO, and PMMA. Thus, the combination of structural and optical characterization methods indicates that PEI, P4VP, and PVP bind to the surface of growing perovskite materials during co-precipitation, promoting the formation of nanocrystals while simultaneously reducing surface defects, which produces photoluminescent composite materials. Therefore, polymers play an active role as polymer macroligands in driving nanocrystal formation by playing a similar function as surface-active ligands in colloidal nanocrystal synthesis.[41] The work reported here establishes new design rules for using polymers with chemical functionalities to promote desired optical properties and will guide perovskite/polymer combinations for improved device performance for applications as LEDs and photodetectors.

Results

$MAPbBr_3$ composite perovskite/polymer nanomaterials at approximately 75 wt% perovskite were prepared using a single, co-precipitation method, while at room temperature. Perovskite precursors (MABr: 0.0280 g per 0.25 mmol and $PbBr_2$, 0.0920 g, 0.25 mmol) and a chosen polymer (PEI: 0.0400 g per 0.40 μmol; PEO: 0.0400 g per 0.40 μmol; P4VP: 0.0400 g per 0.67 μmol; PS: 0.0400 g per 10 μmol; PVP: 0.0400 g per 4.0 μmol; PMMA: 0.0400 g per 3.4 μmol) were dissolved in 2.0 mL *N*,*N*-dimethylformamide (DMF) and then the solution was injected into 5.0 mL toluene, which induces the formation of perovskite materials *via* co-precipitation (Fig. 1a). An approximately 75 wt% perovskite with respect to polymer was chosen as samples prepared in this range demonstrated the greatest fluorescence emission intensity (Fig. S1†). The precipitated perovskite/polymer material (orange/yellow) was collected by centrifugation and dried under vacuum at room temperature overnight (Fig. 1b). The dried powder is easily pressed into a ~1 mm thick wafer (Fig. 1c), which exhibits clear PL response for the nitrogen containing $MAPbBr_3$/PEI perovskite/polymer composite while under UV irradiation (Fig. 1d).[42] It is also possible to form films on a substrate by drop casting a perovskite/polymer composites solution onto the top of a glass substrate followed by annealing at 60 °C for 30 min to accelerate toluene evaporation.

Polymer solubility and polymer/perovskite yields from the co-precipitation process were assessed for all polymer combinations by measuring the total amount of polymer/perovskite precipitate after centrifugation and drying. The polymer yield in the precipitate was determined by assuming that all the perovskite was removed during precipitation and centrifugation, which is supported by the nearly quantitative yield for the neat perovskite sample. Total precipitate and polymer yield values are presented in Table S1.†

PS and P4VP are both soluble in toluene, yet the total polymer percent yields are different. The P4VP sample produced an almost quantitative polymer yield (~100%) after co-precipitation, while PS remained in the toluene solution, leaving only neat perovskite, with ~0% polymer yield. Thus, P4VP/perovskite interactions are stronger than P4VP/toluene interactions. Similarly, both PEI and PEO are soluble in toluene, yet in both samples the majority of polymer precipitates out with the perovskite crystals, ~89% and ~90% respectively. PVP is insoluble in toluene, thus quantitative polymer yield (~100%) is well expected and observed. PMMA is also soluble in toluene, and it was found that PMMA also remained in the toluene solution, similarly to PS with 0% polymer yield. Thus, PVP/toluene interactions are stronger than PMMA/perovskite interactions.

To investigate polymer functional group interactions with perovskite nanocrystals, a set of six chemically diverse poly-

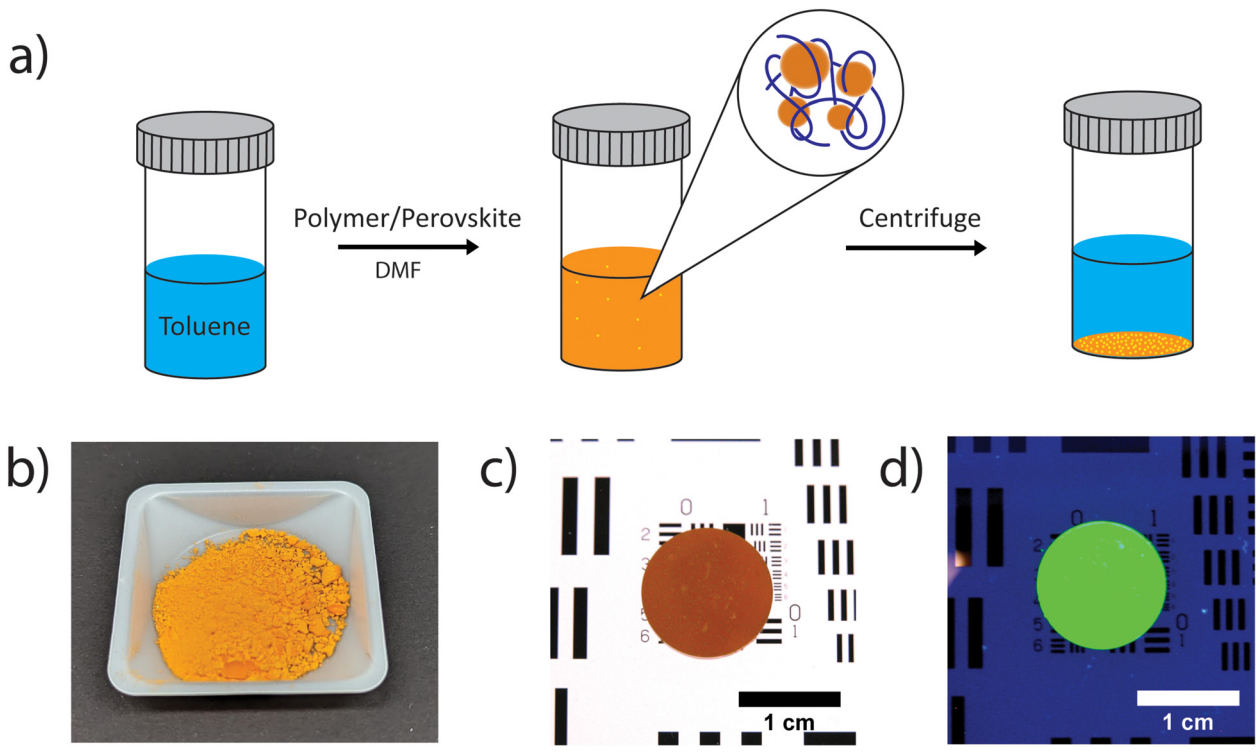

Fig. 1 Overview of composite perovskite/polymer material synthesis *via* co-precipitation and film formation. (a) Perovskite/polymer powders were prepared by co-precipitation. Polymer and perovskite precursors are first dissolved in DMF, injected into toluene, and then separated from the mixture through centrifugation. (b) Resulting perovskite/polymer powders collected after drying. (c) Pressed $MAPbBr_3$/PEI perovskite/polymer powder into a ~1 mm thick wafer under ~300 MPa pressure for 168 h. (d) Resulting perovskite/polymer film excited under 365 nm UV light.

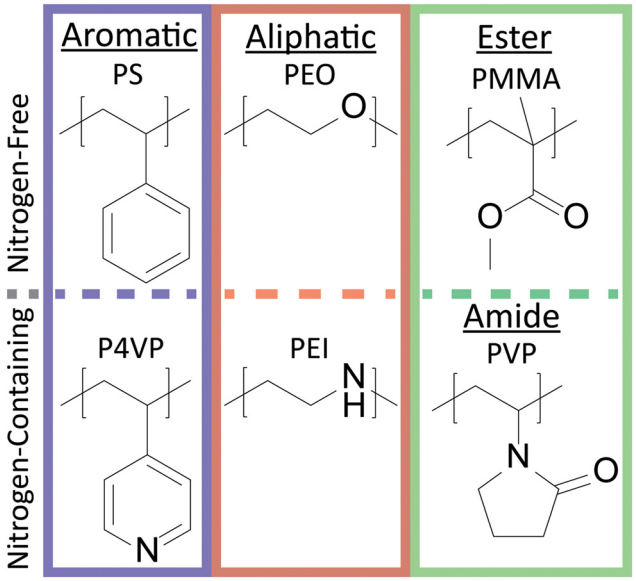

Fig. 2 Chemical structures of polymers used for synthesizing composite perovskite/polymer materials. All polymers are grouped by similar chemical functionalities, which include aromatic, aliphatic, ester, and amide.

mers was utilized (Fig. 2). The functional groups studied were aromatic (PS and P4VP), aliphatic (PEO and PEI), and ester or amide (PMMA and PVP). Within these different functional groups, there was also a clear chemical distinction between polymers containing or not containing nitrogen. Indeed, fluorescence spectroscopy revealed intensity decreased as follows: aliphatic sp^3 N ≈ aromatic sp^2 N > aliphatic sp^3 O in ether > sp^2 phenyl group in PS. Polymer characterization including molecular weight and glass transition temperature are shown in Table S2.†

The optical properties of the composite perovskite materials were first evaluated by photoluminescence measurements. Fig. 3a shows the drastic differences in PL response between the composite films prepared using different polymers when excited using a UV lamp at 365 nm wavelength. The images indicate that perovskite films prepared using PEI, P4VP, and PVP are visually more photoluminescent than perovskite films made with PMMA, PS, and PEO. The neat perovskite film is indicated by $MAPbBr_3$ and shows no visible PL. Next, emission fluorescence spectra were measured to show optical similarities and differences among the films. The fluorescence emission spectrum in Fig. 3b corresponds well with Fig. 3a in that PEI, P4VP, and PVP samples exhibited the strongest photoluminescence, while PMMA, PS, PEO, and $MAPbBr_3$ had mild photoluminescence. Finally, polymer molecular weight does not seem to have a significant impact on the PL signal. Composite materials prepared using PEI with three different molecular weights exhibited emission spectra at similar wavelengths (Fig. S2†).

Photoluminescence among nitrogen-containing polymers (PEI, P4VP, and PVP) were compared with equivalent mole fractions (*i.e.*, 0.59 mole fraction of N to $PbBr_2$), as opposed to weight percent, which were calculated from the initial reagent solution mixture before precipitation (Fig. S3†). In Fig. S3a,† films prepared with nitrogen-containing polymers demonstrated enhanced fluorescence, similar to results shown in Fig. 3a. Emission fluorescence spectra in Fig. 3b for composite samples prepared using PEI, P4VP, and PVP exhibited similar emission wavelengths, but with variation in fluorescence intensity. The differences in fluorescence intensities suggest that there is a balance between Lewis basicity of the N-groups and degree of polymer coverage on the perovskite surface. It is also important to note that the mole fractions of PEI and PEO to $PbBr_2$ are very similar, 0.79 for both, yet the resulting emission fluorescence intensity between the samples is drastically different. Therefore, although the mole fraction of polymer functional groups is important, we posit that the Lewis basicity of the functional groups is more significant.

To further investigate the emissive properties of all perovskite/polymer composites, absolute PLQY measurements were

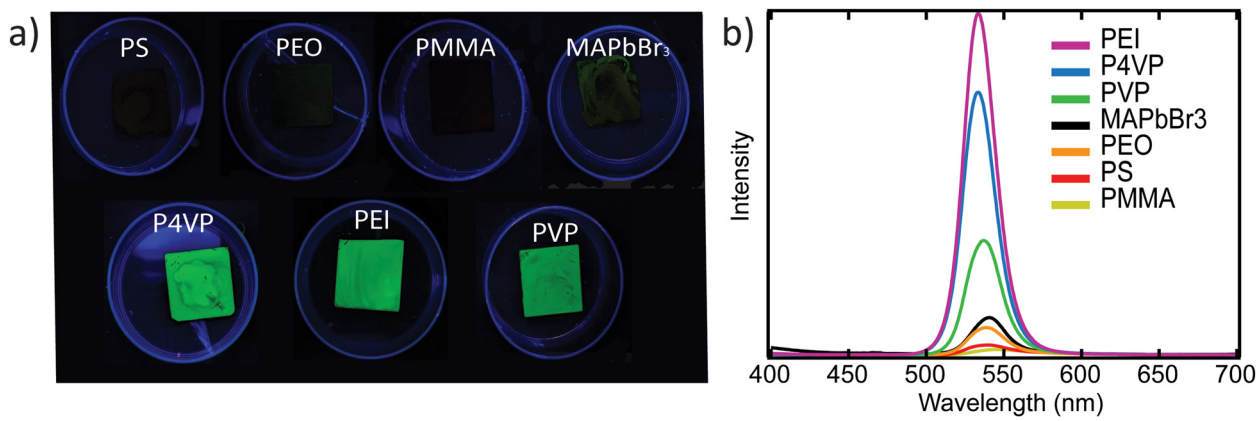

Fig. 3 Emission fluorimetry of perovskite/polymer films under 365 nm excitation. (a) Photographs of photoluminescent perovskite/polymer films on glass irradiated with a 365 nm UV lamp. $MAPbBr_3$ is the pure perovskite material prepared by the precipitation method without polymer. (b) Fluorescence emission spectra of perovskite/polymer films excited with 365 nm wavelength.

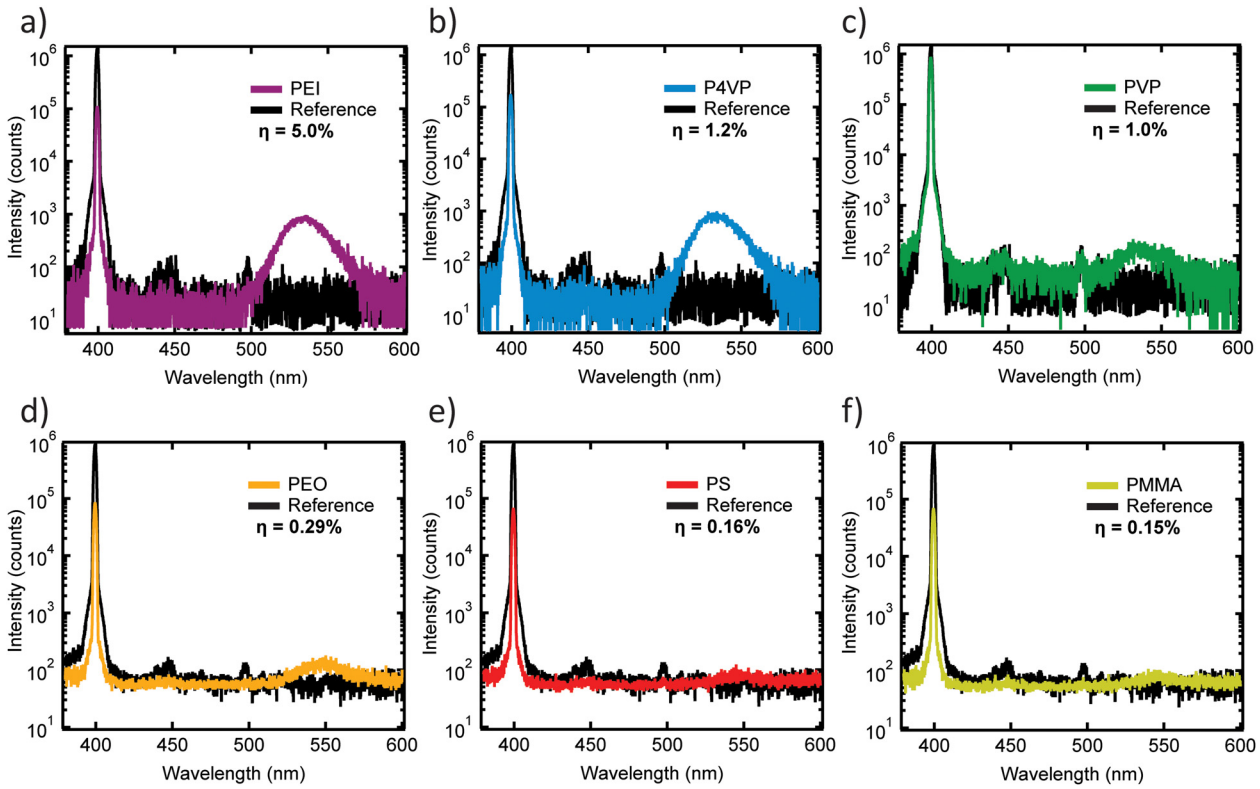

Fig. 4 Absolute PLQY measurements of polymer perovskite films, excited at 400 nm. Absolute QY of the composite material made with PEI (a), PVP (b), P4VP (c), PEO (d), PS (e), and PMMA (f), excited at 400 nm.

performed on drop-cast films. Fig. 4 plot emission spectra for each film (colored lines) and blank glass slides (black lines) with excitation at 400 nm. Absolute PLQY values (η) are provided within each panel. Note that η values are low due to significant reabsorption in the several micrometer-thick films (see absorbance spectra in Fig. S4a†). Nonetheless, the results reveal that $MAPbBr_3$/PEI composite films at ~75 wt% are the brightest in comparison to films prepared with other nitrogen-containing polymers P4VP or PVP. PLQY values for composite samples prepared with nitrogen-containing polymers (Fig. 4a and b) are significantly higher than PLQY values of samples prepared with nitrogen-absent polymers (Fig. 4d and f). Higher PLQY indicates better passivation of the perovskite surface with a reduced number of trap states that enhance resulting emission. Overall, the results in Fig. 3 and 4 indicate that samples synthesized with nitrogen-containing polymers are brighter than samples synthesized with polymers without nitrogen.

Transmission electron microscopy (TEM) and X-ray diffraction (XRD) confirmed that the composite perovskite/polymer materials were indeed crystalline and exhibited the same structure irrespective of polymer choice (Fig. 5). TEM images indicate that bulk crystalline features were present in all composite samples, specifically 269 ± 100 nm in neat $MAPbBr_3$, 136 ± 28 nm in PS samples, 144 ± 44 nm in PEI samples, 121 ± 51 nm in P4VP samples, 184 ± 38 nm in PVP samples, and 257 ± 74 in PEO samples. Further, samples synthesized with nitrogen-containing polymers and PEO showed additional nanocrystalline features, 7.9 ± 2.9 nm in PEI samples, 9.8 ± 3.2 nm in P4VP samples, 8.4 ± 1.9 nm in PVP samples, and 4.2 ± 0.9 nm in PEO samples. For perovskite/polymer composites made with nitrogen-containing polymers, functional groups lead to the formation of nanocrystalline features, as shown at higher resolution images in PEI, P4VP, and PVP samples (Fig. 5b, f and j). Fig. 5b, f and j display the presence of nanoscale particles with an amorphous media around them where the amorphous region is the polymer matrix encapsulating the perovskite material. For the PS and PMMA sample (Fig. 5c, d, k and l), the crystals formed larger domain sizes as compared to the sample with PEI, P4VP, and PVP and are comparable to the neat $MAPbBr_3$ perovskite crystals (Fig. S5a and b†). It is important to mention that even though there are minor changes in photoluminescence with respect to PEI molecular weight (Fig. S2†), there is the potential for changes to the nanocrystal size and morphology. Additionally, the X-ray diffraction (XRD) patterns for all composite samples (Fig. 5m) confirmed the presence of perovskite crystal structure with strong bulk crystal signals. Interestingly, the set of films displays near identical XRD patterns, yet, they have distinctly different optical properties. Increased PL could potentially be due to the presence of nanocrystalline features in the samples prepared with PEI, P4VP, and PVP,[43,44] but composite samples prepared

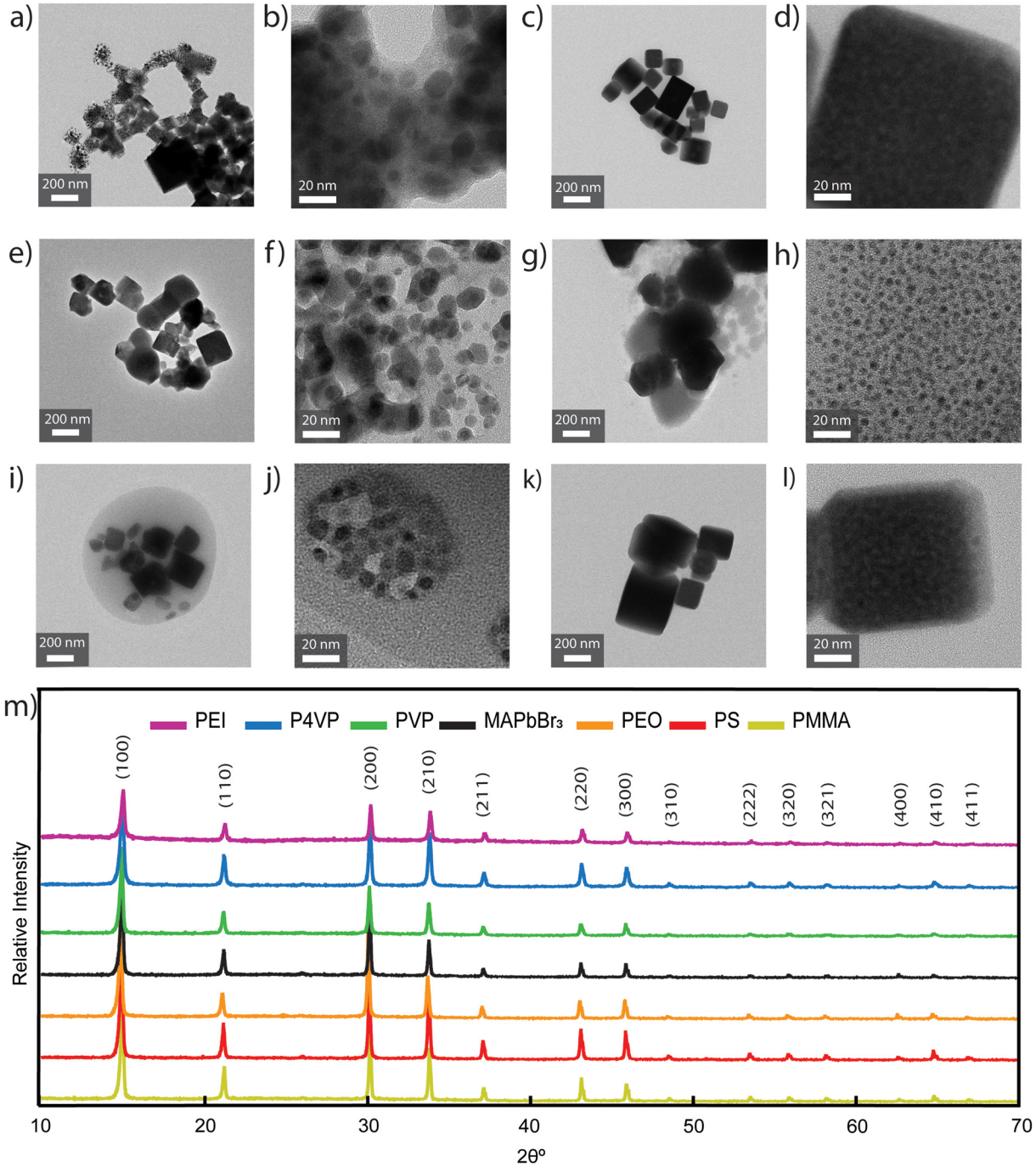

Fig. 5 TEM images and XRD patterns of synthesized perovskite/polymer materials. TEM images of composite perovskite films made with (a), (b) P4VP, (c, d) PS, (e, f) PEI, (g, h) PEO, (i, j) PVP, and (k), (l) PMMA. Samples were prepared by drop casting the precipitate solution on TEM grids and vacuum drying overnight. (m) XRD patterns of perovskite/polymer materials, Miller indices are used to index the $MAPbBr_3$ crystal structure.

with PEO also have nanoscale particles (Fig. 5g and h) yet exhibit reduced PL (Fig. 3a). Therefore, the enhanced PL is attributed due to perovskite/polymer surface interactions. Strong interactions could be the result of polymers binding to surface defects of the nanocrystal, which would passivate the surface.

Perovskite/polymer surface interactions were determined by comparing Fourier-transform infrared spectroscopy (FTIR) spectra for composite perovskite/polymer composite films and the individual perovskite and polymer components (Fig. 6a–h). Scans were performed with a resolution of 4 cm^{-1} with 400 scan repeats in the 4000–500 cm^{-1} range. For each polymer sample, chemically relevant frequency ranges were chosen for peak shift analysis. Specifically, the C–N stretch at 1136 cm^{-1} for PEI (Fig. 6a and e), the C═O stretch at 1651 cm^{-1} for PVP (Fig. 6b and f), the C–N stretch at 1068.5 cm^{-1} for P4VP

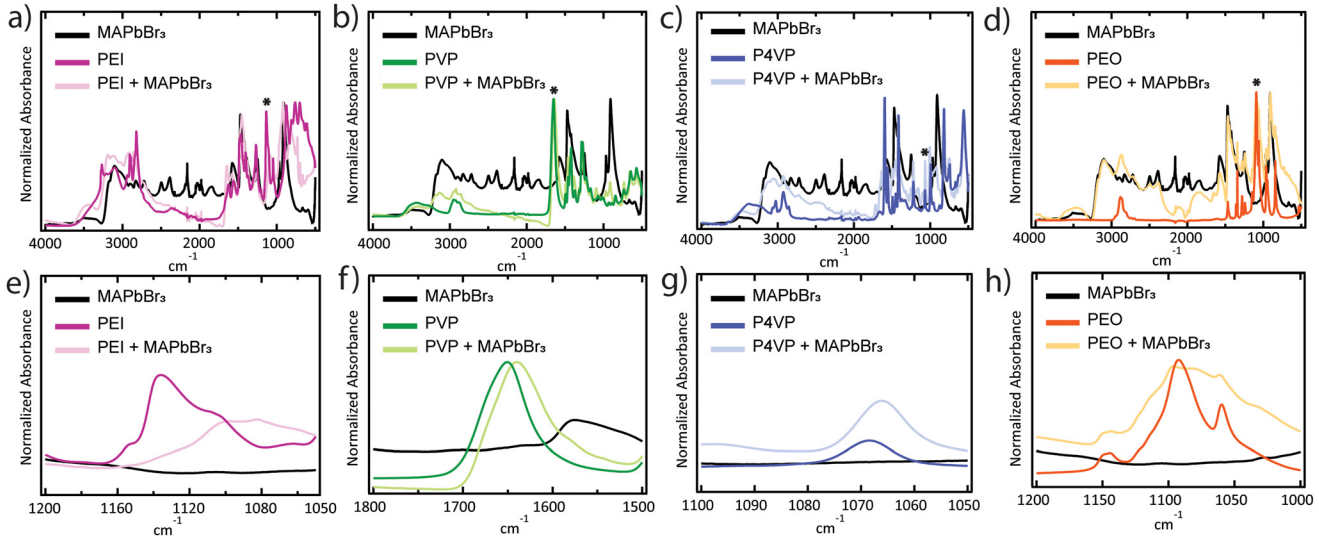

Fig. 6 FTIR spectra of composite materials and individual perovskite and polymer components. Spectra of neat $MAPbBr_3$ samples compared to FTIR spectra of neat polymers PEI, PVP, P4VP, and PEO, and the corresponding perovskite/polymer composite samples. (a–d) Show the full spectra where (e–h) are in a narrow range to highlight peaks of interest for the C–N stretch in PEI, the C=O stretch in PVP, the C–N stretch in P4VP, and the C–O stretch in PEO.

(Fig. 6c and g), and the C–O stretch at 1092 cm^{-1} for PEO (Fig. 6d and h). FTIR scans of samples prepared with PMMA and PS are shown in Fig. S6.† All peaks corresponding to polymer-related stretches shifted to lower frequencies for the perovskite/polymer composite samples. Peaks shifted to 1101 cm^{-1}, 1640 cm^{-1}, 1066 cm^{-1}, and 1082 cm^{-1} and broadened for PEI, PVP, P4VP, and PEO composites, respectively. These are evidence of interactions between the functional groups in the polymers and crystal surface.[45] Even though the shift in the peak is observed in chosen samples, the final photoluminescence does not correspond to the shifts, which means that interactions alone are not the primary source of strong photoluminescence. The shift in the PEO composite samples is yet another evidence suggesting that the final photoluminescence is not impacted by interactions alone because of the absence of photoluminescence in the composite films (Fig. 3a and b).

Discussion

The combination of the characterization results from PLQY, TEM, XRD and FTIR indicate that the surface passivation by nitrogen-containing polymers increases the PL of perovskite composite materials, and is attributed to nitrogen coordination with under-coordinated lead ions on the perovskite crystal surface.[46] Thus, the functional groups contained in the polymer macroligands passivate perovskite crystal surface defects and/or trap sites, which significantly decrease the nonradiative recombination by substantially reducing the trap density.[44] Additionally, PLQY measurements suggest that polymer passivation positively affects the emission.[47] An example of reduced nonradiative charge recombination has been reported by Wang *et al.* where the traps of Pb antisites in a $MAPbI_3$ perovskite crystal were passivated by small nitrogen-containing molecules, and as a result, the power conversion efficiency of the passivated photovoltaic devices increased up to 22.6%.[48] Passivation of Pb antisites by nitrogen-containing polymers is also suggested for nanocrystalline $MAPbBr_3$.[49] In a different example, reported by Wang *et al.*, formamidinium lead triiodide ($FAPbI_3$) perovskite crystals were passivated by benzilamines, nitrogen-containing small molecules, which improved water stability and the resulting electronic performance.[50] Here, we predict that nitrogen-containing polymers with functional groups that preferentially interact with perovskite surfaces will actively passivate surface defects during material synthesis (Fig. 7).

It is important to discuss the presence of nanocrystals in composite materials synthesized with PEO and the resulting absence of PL, as compared to PEI. Even though both composite materials exhibit the presence of nanocrystals, only samples made with PEI have enhanced PL when compared to PEO. We suggest that the enhanced PL of PEI samples results from the strong passivation of the trap states on the perovskite crystal surface because nitrogen atoms coordinate with under-coordinated Pb ions on the crystal surface. Strong passivation of surface traps is primary reason for samples prepared with PEI to have strong photoluminescence. In contrast, PEO is a weaker passivating agent because oxygen atoms are weaker Lewis bases than nitrogen atoms in PEI. Ultimately, the strength of polymer passivation is responsible for the resulting photoluminescence.[51]

As shown in Fig. 3 and 4, samples prepared with PEI exhibit the highest fluorescence, followed by P4VP, and then

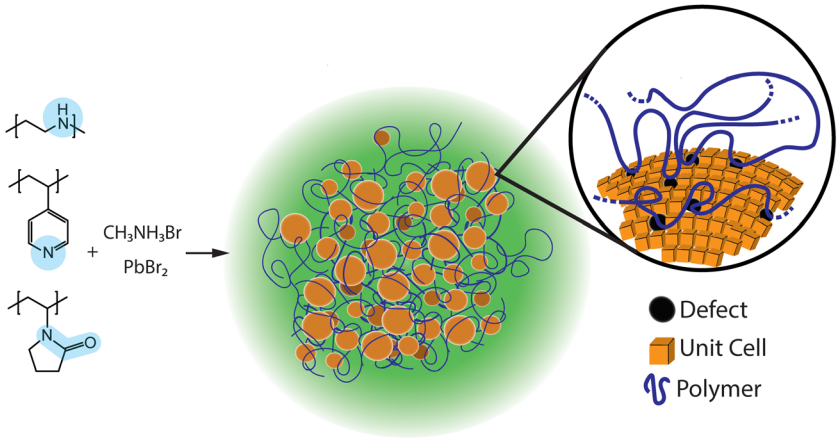

Fig. 7 Schematic of polymer macroligand encapsulation of perovskite nanocrystals. The prediction is such that nitrogen-containing polymers will strongly bind to the crystal surface, passivating the trap sites that form during synthesis.

finally PVP. From the photoluminescence studies at 75 wt% perovskite, PEI must have better passivation efficiency and therefore decrease trap density on the perovskite crystal as compared to P4VP and PVP. Indeed, analysis of FTIR absorbances before and after adding polymer to the perovskite, confirms a significant interaction between the C–N bond in PEI and perovskite. However, if the samples are prepared at an equivalent 0.59 mole fraction of N to $PbBr_2$, P4VP exhibits the highest PL (Fig. S3 and S7†). At the equivalent mole fraction, P4VP sample exhibited the highest QY of 2.6% as compared to PVP and PEI with QY of 1.7% and 1.3%, respectively. P4VP is a stronger Lewis base than PVP, which is evident in the PLQY measurements. However, P4VP is a weaker Lewis base compared to PEI and is expected to exhibit a weaker PL response based on passivation strength, but that is not evident. The exact reason for why P4VP has a greater PLQY than PEI at constant mole fraction is not currently known. One possibility is that the polymer surface coverage on the perovskite could be different. In addition, time-resolved PL studies were conducted on nitrogen-containing samples to investigate photoluminescence kinetics of composite films (Fig. S4b†). Table S3† gives the biexponential fit parameters for each curve. PEI PL decay data showed monoexponential-like behavior (*i.e.* A_1 is ~4× larger A_2 as compared to the other polymers where $A_1 = A_2$,) and fast lifetime (~10 ns), as compared to lifetimes of P4VP and PVP, which agrees with previously reported, highly luminescent halide perovskite. PVP and P4VP samples showed a pronounced biexponential-like behavior, dissimilar to PEI.[52] The presence of significant fast and slow decays in P4VP and PVP samples complicates further comparison between photoluminescence kinetics because multiple mechanisms, such as trap-induced recombination and reabsorption, could be present but not fully differentiated.

As demonstrated here, polymers will act as macroligands by inducing the formation of nanoscale particles and passivating surface defects, similar to how small molecule ligands, such as octylamine, oleylamine, didodecylamine, phosphenes, various acids, and zwitterions are used to make colloidal perovskite nanocrystals.[16,18,19,53] Similarly, peptides are known to be active in biomineralization processes and metal nanocrystal synthesis.[54–57] In both of these examples, peptides are macromolecules that act as surface active agents that control inorganic material growth. Surface-active ligands are necessary components in the synthesis of high-quality nanocrystals.[58,59] High surface coverage of ligands passivates the nanocrystal surface and prevents agglomeration, which significantly reduces surface trap density and non-radiative recombination.[60,61] Thus, in composite polymer materials, translating knowledge regarding ligand chemistry to synthetic polymers will potentially transform current methods for creating polymer/inorganic composite materials. The results shown here are the first demonstration that polymers with repeat units of similar chemical functionalities as established surface-active ligands play the role of polymer macroligand. The term "polymer macroligand" has previously been designated to telechelic polymers that typically contain pyridine, bipyridine, or terpyridine functionality at the end of the polymer chain and will specifically bind to metals from polymer–metal complexes.[60,62–64] Therefore, the work reported here expands the possibilities of polymer macroligands to include polymers that have chemical functionality in the repeat unit that will strongly interact with crystal surfaces.

Conclusion

Here, we present a one-step synthesis procedure for composite perovskite/polymer materials and show that the polymer chemical composition directly affects the optical properties of OIP composite materials. We predicted that polymers would passivate perovskite crystal surface traps as well as induce the formation of nanocrystals. Experiments were designed and conducted to characterize the emissive properties of perovskite/polymer materials and systematically test the effect from

polymers with different chemical functionalities. The results confirm that perovskite materials synthesized with nitrogen-containing polymer matrices (PEI, P4VP, and PVP) exhibit enhanced photoluminescence as compared to nitrogen-absent polymers (PS, PEO, and PMMA), due to nitrogen coordination with under-coordinated lead ions on perovskite crystal surface. The strong passivation of polymers in perovskite surfaces stabilizes the nanocrystalline features in solution as the crystals form as well as reduces the number of defects which promote photoluminescence. We envision that the work reported here will open new pathways for applying polymers with crystal systems beyond hybrid halide perovskite. The understanding of polymer macroligand effects will provide a new, facile, and scalable synthesis of high-quality composite perovskite materials with superior photoluminescence properties for displays, LEDs, lasers, or optical sensors.

Experimental section

Materials

Poly(methyl methacrylate) (PMMA, M_w = 11 600 g mol^{-1}), poly (vinylpyrrolidone) (PVP, M_w = 10 000 g mol^{-1}), poly(ethylene oxide) (PEO, M_w = 100 000 g mol^{-1}), poly(4-vinylpyridine) (P4VP, M_w = 60 000 g mol^{-1}), $PbBr_2$ (≥98%), and MABr (≥99%, anhydrous), styrene monomer with 4-*tert*-butylcatechol as a stabilizer (≥99%), 2-cyano-2-propyl dodecyl trithiocarbonate (97% (HPLC)), 2,2′-azobis(2-methylpropionitrile) (98%), activated aluminum oxide, and methanol (≥99.8%) were purchased from Sigma-Aldrich and used as received. Poly(ethylenimine) polymers (PEI, M_w = 2500 g mol^{-1}, 100 000 g mol^{-1}, and 250 000 g mol^{-1}) were purchased from Polysciences, Inc. and used as received. Poly(styrene) (PS) was synthesized *via* reversible addition–fragmentation chain transfer (RAFT) polymerization.[65] Perovskite/polymer solutions were prepared using *N*,*N*-dimethylformamide (99.7+%) from Alfa Aesar, and toluene from Fisher Chemical.

Poly(styrene) synthesis

Styrene monomer was purified through an activated aluminum oxide powder column. For the PS synthesis: 48.0 mmol of styrene monomer, 0.20 mmol of initiator 2,2′-azobis(2-methylpropionitrile) (AIBN), and 0.80 mmol RAFT agent 2-cyano-2-propyl dodecyl trithiocarbonate were added to 6 mL of toluene in a 100 mL round bottom flask. The mixture was sealed with a septum and sparged with argon for 30 min. The resulting mixture was then heated at 70 °C for 22 h on a temperature-controlled heating plate. The resulting polymer was terminated by introducing air. The polymer was precipitated in methanol and redissolved in toluene three times for purification. The final precipitate was dried in a vacuum oven at room temperature overnight.

Polymer characterization

Synthesized PS was characterized using SEC (Tosoh Bioscience EcoSEC) using tetrahydrofuran as the mobile phase, with a concentration of 5 mg mL^{-1} at 40 °C (Fig. S8†). A TA Instruments Q2000 DSC was used to perform differential scanning calorimetry. To prepare samples, a polymer was added to a DSC pan, made by DSC Consumables, and hermetically sealed. A reference (empty) pan was also prepared. Polymers were heated first at 20 °C min^{-1} to 150 °C, cooled at 10 °C min^{-1} to 30 °C (except PEO, which was cooled to 0 °C), and heated again at 10 °C min^{-1} to 150 °C. After each step, the sample was held for 10 min at the target temperature. Polymer molecular weights and glass transition temperatures (T_g) are shown in Table S2.†

Perovskite/polymer film preparation

Films were fabricated by precipitating the precursor solution containing polymers in an antisolvent and using that precipitate to drop cast on cleaned glass slides. First, the perovskite precursor solutions were prepared by dissolving methylammonium bromide (MABr: 0.0280 g per 0.2501 mmol), lead bromide ($PbBr_2$, 0.0920 g, 0.2507 mmol), and a chosen polymer (PEI: 0.0400 g per 0.40 μmol; PEO: 0.0400 g per 0.40 μmol; P_4VP: 0.0400 g per 0.67 μmol; PS: 0.0400 g per 10 μmol; PVP: 0.0400 g per 4.0 μmol; PMMA: 3.4 μmol) in 2.0 mL of *N*,*N*-dimethylformamide (DMF) in a 7 mL scintillation vial. The precursor solution was thoroughly mixed. Then, 0.5 mL solution was injected into 5.0 mL of an antisolvent, toluene. The solution was centrifuged at 10 000 rpm for 5 min to separate the supernatant and the precipitate. The supernatant was discarded, and the precipitate was mixed with 1 mL of fresh toluene to produce a highly concentrated dispersed perovskite solution. Perovskite solution was then drop-casted on clean glass slides and put on a hot plate at 60 °C for 20 min to allow toluene to evaporate. Glass slides were cleaned by scrubbing with soap and water, sonicated twice for 20 min, first in a beaker of acetone and then in a beaker of isopropanol, and finally treated with UV-Ozone. With the synthesis procedure, the largest weight of the final product attempted was measured to be up to ~7 g.

Material characterization

Film samples were characterized with a Photon Technology International Fluorometer. A clean substrate was used for background subtraction. Fluorescence measurements were conducted by exciting the samples at 365 nm and recording the emission from 400 to 700 nm with a 0.5 nm step and integration time of 0.5 s. Film X-ray diffraction measurements were obtained using a Malvern-Panalytical Empyrean-2 four-circle X-ray diffractometer with a Copper K-α X-ray source over a 2θ range of 10 to 70° with a step of 0.02. TEM images were taken by Tecnai G2 20 XTWIN with LAB_6 as the thermal electron source. All TEM samples were dried in a vacuum at room temperature before measurements. Particle analysis was done through ImageJ software. FTIR measurements were performed on Vertex 70 instrument by Bruker from 4000 to 500 cm^{-1}, with all samples dried overnight in a vacuum at room temperature. The method for FTIR measurements included 100 sample and background scans with 1 cm^{-1} resolution.

A FLS1000 fluorimeter from Edinburgh Instruments (Livingston, Scotland) was employed for absolute PLQY measurements. Tunable excitation was generated with a 450 W Xe arc lamp and a double grating Czerny-Turner monochromator (focal length: 2 × 325 mm). The emission monochromator was a single grating Czerny-Turner monochromator (focal length: 325 mm) and the detector was a photomultiplier tube (PMT) with an in-housing cooling unit operated at −22 °C. Absolute QY values were determined using an integrating sphere compatible with the FLS1000 system. Emission for QY measurements was induced with an excitation bandwidth of 1.5 nm. Emission bandwidths were adjusted until ~1 million counts were observed at the PMT for the glass slide blank at an excitation wavelength of 400 nm and ranged from 0.2 to 0.5 nm depending on the sample. Specimen photoluminescence was collected from 600 nm down to 10 nm below the excitation wavelength with a 0.1 nm step size. η values were determined using Fluoracle software.

Data availability

Data for this article, including .csv files are available at Data Commons at Penn State at **https://doi.org/10.26208/WMY8-B047**.

Conflicts of interest

There are no conflicts to declare.

Acknowledgements

This work is supported by the Air Force Office of Scientific Research (AFOSR) (YIP Award 18RT0680/FA9550-19-1-0047 and 22RT0809/FA9550-22-1-0546). TEM and FT-IR measurements were taken at the Materials Characterization Lab (MCL) in the Materials Research Institute (MRI) at Penn State University. M. C. B and T. A. G. acknowledge the support of Air Force Office of Scientific Research grant number 23RXCOR023 and AFRL/RXEP contract FA8650-22-D-5408.

References

1 A. Dey, J. Ye, A. De, E. Debroye, S. K. Ha, E. Bladt, A. S. Kshirsagar, Z. Wang, J. Yin, Y. Wang, *et al.*, State of the Art and Prospects for Halide Perovskite Nanocrystals, *ACS Nano*, 2021, **15**, 10775–10981, DOI: **10.1021/acsnano.0c08903**.

2 J. Burschka, N. Pellet, S.-J. Moon, R. Humphry-Baker, P. Gao, M. K. Nazeeruddin and M. Grätzel, Sequential deposition as a route to high-performance perovskite-sensitized solar cells, *Nature*, 2013, **499**, 316–319, DOI: **10.1038/nature12340**.

3 M. M. Lee, J. Teuscher, T. Miyasaka, T. N. Murakami and H. J. Snaith, Efficient Hybrid Solar Cells Based on Meso-Superstructured Organometal Halide Perovskites, *Science*, 2012, **338**, 643–647, DOI: **10.1126/science.1228604**.

4 X. Li, D. Bi, C. Yi, J.-D. Décoppet, J. Luo, S. M. Zakeeruddin, A. Hagfeldt and M. Grätzel, A vacuum flash–assisted solution process for high-efficiency large-area perovskite solar cells, *Science*, 2016, **353**, 58–62, DOI: **10.1126/science.aaf8060**.

5 E. Edwardes Moore, V. Andrei, S. Zacarias, I. A. C. Pereira and E. Reisner, Integration of a Hydrogenase in a Lead Halide Perovskite Photoelectrode for Tandem Solar Water Splitting, *ACS Energy Lett.*, 2020, **5**, 232–237, DOI: **10.1021/acsenergylett.9b02437**.

6 L. Dou, Y. Yang, J. You, Z. Hong, W.-H. Chang, G. Li and Y. Yang, Solution-processed hybrid perovskite photodetectors with high detectivity, *Nat. Commun.*, 2014, **5**, 5404.

7 Y. Lee, J. Kwon, E. Hwang, C.-H. Ra, W. J. Yoo, J.-H. Ahn, J. H. Park and J. H. Cho, High-Performance Perovskite–Graphene Hybrid Photodetector, *Adv. Mater.*, 2015, **27**, 41–46, DOI: **10.1038/ncomms6404**.

8 W. Chen, M. Zhou, Y. Liu, X. Yu, C. Pi, Z. Yang, H. Zhang, Z. Liu, T. Wang, J. Qiu, S. F. Yu, Y. Yang and X. Xu, All-Inorganic Perovskite Polymer–Ceramics for Flexible and Refreshable X-Ray Imaging, *Adv. Funct. Mater.*, 2022, **32**, 2107424, DOI: **10.1002/adfm.202107424**.

9 L. Protesescu, S. Yankunin, M. I. Bodnarchuk, F. Krieg, R. Caputo, C. H. Hendon, R. X. Yang, A. Walsh and M. V. Kovalenko, Nanocrystals of Cesium Lead Halide Perovskite ($CsPbX_3$, X = Cl, Br, and I): Novel Optoelectronic Materials Showing Bright Emission with Wide Color Gamut, *Nano Lett.*, 2015, **15**, 3692–3696, DOI: **10.1021/nl5048779**.

10 Y. Shang, Y. Liao, Q. Wei, Z. Wang, B. Xiang, Y. Ke, W. Liu and Z. Ning, Highly stable hybrid perovskite light-emitting diodes based on Dion-Jacobson structure, *Sci. Adv.*, 2019, **5**, eaaw8072, DOI: **10.1126/sciadv.aaw8072**.

11 H.-C. Wang, Z. Bao, H.-Y. Tsai, A.-C. Tang and R.-S. Liu, Perovskite Quantum Dots and Their Application in Light-Emitting Diodes, *Small*, 2018, **14**, 1702433, DOI: **10.1002/smll.201702433**.

12 X. Li, Z. Wen, S. Ding, F. Fang, B. Xu, J. Sun, C. Liu, K. Wang and X. W. Sun, Facile In Situ Fabrication of $Cs_4PbBr_6/CsPbBr_3$ Nanocomposite Containing Polymer Films for Ultrawide Color Gamut Displays, *Adv. Opt. Mater.*, 2020, **8**, 2000232, DOI: **10.1002/adom.202000232**.

13 F. Zhang, H. Zhong, C. Chen, X.-g. Wu, X. Hu, H. Huang, J. Han, B. Zou and Y. Dong, Brightly Luminescent and Color-Tunable Colloidal $CH_3NH_3PbX_3$ (X = Br, I, Cl) Quantum Dots: Potential Alternatives for Display Technology, *ACS Nano*, 2015, **9**, 4533–4542, DOI: **10.1021/acsnano.5b01154**.

14 G. Xing, N. Mathews, S. Sun, S. S. Lim, Y. M. Lam, M. Grätzel, S. Mhaisalkar and T. C. Sum, Long-Range Balanced Electron- and Hole-Transport Lengths in Organic-

Inorganic $CH_3NH_3PbI_3$, *Science*, 2013, **342**, 344–347, DOI: 10.1126/science.1243.

15 J.-H. Im, C.-R. Lee, J.-W. Lee, S.-W. Park and N.-G. Park, 6.5% efficient perovskite quantum-dot-sensitized solar cell, *Nanoscale*, 2011, **3**, 4088–4093, DOI: 10.1039/C1NR10867K.

16 F. Liu, Y. Zhang, C. Ding, S. Kobayashi, T. Izuishi, N. Nakazawa, T. Toyoda, T. Ohta, S. Hayase, T. Minemoto, K. Yoshino, S. Dai and Q. Shen, Highly Luminescent Phase-Stable $CsPbI_3$ Perovskite Quantum Dots Achieving Near 100% Absolute Photoluminescence Quantum Yield, *ACS Nano*, 2017, **11**, 10373–10383, DOI: 10.1021/acsnano.7b05442.

17 H. J. Snaith, Present status and future prospects of perovskite photovoltaics, *Nat. Mater.*, 2018, **17**, 372–376, DOI: 10.1038/s41563-018-0071-z.

18 A. Pan, B. He, X. Fan, Z. Liu, J. J. Urban, A. P. Alivisatos, L. He and Y. Liu, Insight into the Ligand-Mediated Synthesis of Colloidal $CsPbBr_3$ Perovskite Nanocrystals: The Role of Organic Acid, Base, and Cesium Precursors, *ACS Nano*, 2016, **10**(8), 7943–7954, DOI: 10.1021/acsnano.6b03863.

19 F. Krieg, S. T. Ochsenbein, S. Yakunin, S. T. Brinck, P. Aellen, A. Süess, B. Clerc, D. Guggisberg, O. Nazarenko, Y. Shynkarenko, S. Kumar, C. J. Shih, I. Infante and M. V. Kovalenko, Colloidal $CsPbX_3$ (X = Cl, Br, I) Nanocrystals 2.0: Zwitterionic Capping Ligands for Improved Durability and Stability, *ACS Energy Lett.*, 2018, **3**(3), 641–646, DOI: 10.1021/acsenergylett.8b00035.

20 S. F. Solari, S. Kumar, J. Jagielski, N. M. Kubo, F. Krumeich and C. Shih, Ligand-assisted solid phase synthesis of mixed-halide perovskite nanocrystals for color-pure and efficient electroluminescence, *J. Mater. Chem. C*, 2021, **9**, 5771–5778, DOI: 10.1039/D0TC04667A.

21 A. J. Prochazkova, M. C. Scharber, C. Yumusak, *et al.*, Synthesis conditions influencing formation of $MAPbBr_3$ perovskite nanoparticles prepared by the ligand-assisted precipitation method, *Sci. Rep.*, 2020, **10**, 15720, DOI: 10.1038/s41598-020-72826-6.

22 J. D. Roo, M. Ibáñez, P. Geiregat, G. Nedelcu, W. Walravens, J. Maes, J. C. Martins, I. V. Driessche, M. V. Kovalenko and Z. Hens, Highly Dynamic Ligand Binding and Light Absorption Coefficient of Cesium Lead Bromide Perovskite Nanocrystals, *ACS Nano*, 2016, **10**(2), 2071–2081, DOI: 10.1021/acsnano.5b06295.

23 Y. J. Yoon, Y. Chang, S. Zhang, M. Zhang, S. Pan, Y. He, C. H. Lin, S. Yu, Y. Chen, Z. Wang, Y. Ding, J. Jung, N. Thadhani, V. V. Tsukruk, Z. Kang and Z. Lin, Enabling Tailorable Optical Properties and Markedly Enhanced Stability of Perovskite Quantum Dots by Permanently Ligating with Polymer Hairs, *Adv. Mater.*, 2019, **31**, 1901602, DOI: 10.1002/adma.201901602.

24 S. Wang, L. Du, Z. Jin, Y. Xin and H. Mattoussi, Enhanced Stabilization and Easy Phase Transfer of $CsPbBr_3$ Perovskite Quantum Dots Promoted by High-Affinity Polyzwitterionic Ligands, *J. Am. Chem. Soc.*, 2020, **142**(29), 12669–12680.

25 F. Wang, A. Shimazaki, F. Yang, K. Kanahashi, K. Matsuki, Y. Miyauchi, T. Takenobu, A. Wakamiya, Y. Murata and K. Matsuda, Highly Efficient and Stable Perovskite Solar Cells by Interfacial Engineering Using Solution-Processed Polymer Layer, *J. Phys. Chem. C*, 2017, **121**, 1562–1568, DOI: 10.1021/acs.jpcc.6b12137.

26 J. Wu, Y. Cui, B. Yu, K. Liu, Y. Li, H. Li, J. Shi, H. Wu, Y. Luo, D. Li and Q. Meng, A Simple Way to Simultaneously Release the Interface Stress and Realize the Inner Encapsulation for Highly Efficient and Stable Perovskite Solar Cells, *Adv. Funct. Mater.*, 2019, **29**, 1905336, DOI: 10.1002/adfm.201905336.

27 S. N. Habisreutinger, T. Leijtens, G. E. Eperon, S. D. Stranks, R. J. Nicholas and H. J. Snaith, Carbon Nanotube/Polymer Composites as a Highly Stable Hole Collection Layer in Perovskite Solar Cells, *Nano Lett.*, 2014, **14**, 5561–5568, DOI: 10.1021/nl501982b.

28 Y. Wang, J. He, H. Chen, J. Chen, R. Zhu, P. Ma, A. Towers, Y. Lin, A. J. Gesquiere, S.-T. Wu and Y. Dong, Ultrastable, Highly Luminescent Organic–Inorganic Perovskite–Polymer Composite Films, *Adv. Mater.*, 2016, **28**, 10710–10717, DOI: 10.1002/adma.201603964.

29 Y. Wei, X. R. Deng, Z. X. Xie, X. C. Cai, S. S. Liang, P. A. Ma, Z. Y. Hou, Z. Y. Cheng and J. Lin, Enhancing the Stability of Perovskite Quantum Dots by Encapsulation in Crosslinked Polystyrene Beads via a Swelling–Shrinking Strategy toward Superior Water Resistance, *Adv. Funct. Mater.*, 2017, **27**, 1703535, DOI: 10.1002/adfm.201703535.

30 T. Xuan, J. Huang, H. Liu, S. Lou, L. Cao, W. Gan, R. Liu and J. Wang, Super-Hydrophobic Cesium Lead Halide Perovskite Quantum Dot-Polymer Composites with High Stability and Luminescent Efficiency for Wide Color Gamut White Light-Emitting Diodes, *Chem. Mater.*, 2019, **31**(3), 1042–1047, DOI: 10.1021/acs.chemmater.8b04596.

31 P. G. Papagiorgis, A. Manoli, A. Alexiou, P. Karacosta, X. Karagiorgis, G. Papaparaskeva, C. Bernasconi, M. I. Bodnarchuk, M. V. Kovalenko, T. Krasia-Christoforou and G. Itskos, Robust Hydrophobic and Hydrophilic Polymer Fibers Sensitized by Inorganic and Hybrid Lead Halide Perovskite Nanocrystal Emitters, *Front. Chem.*, 2019, **7**, 1–12, DOI: 10.3389/fchem.2019.00087.

32 Q. Zhou, Z. Bai, W. G. Lu, Y. Wang, B. Zou and H. Zhong, In Situ Fabrication of Halide Perovskite Nanocrystal-Embedded Polymer Composite Films with Enhanced Photoluminescence for Display Backlights, *Adv. Mater.*, 2016, **28**, 9163–9168, DOI: 10.1002/adma.201602651.

33 K. Wang, L. Zheng, T. Zhu, L. Liu, M. L. Becker and X. Gong, High performance perovskites solar cells by hybrid perovskites co-crystallized with poly(ethylene oxide), *Nano Energy*, 2020, **67**, 104229, DOI: 10.1016/j.nanoen.2019.104229.

34 T.-H. Han, J.-W. Lee, C. Choi, S. Tan, C. Lee, Y. Zhao, Z. Dai, N. De Marco, S.-J. Lee, S.-H. Bae, Y. Yuan, H. M. Lee, Y. Huang and Y. Yang, Perovskite-Polymer Composite Cross-Linker Approach for Highly-Stable and Efficient Perovskite Solar Cells, *Nat. Commun.*, 2019, **10**, 520, DOI: 10.1038/s41467-019-08455-z.

35 T. Xu, Y. Meng, M. Wang, M. Li, M. Ahmadi, Z. Xiong, S. Yan, P. Chen and B. Hu, Poly(ethylene oxide)-assisted energy funneling for efficient perovskite light emission, *J. Mater. Chem. C*, 2019, **7**, 8287–8293, DOI: **10.1039/C9TC01906E**.

36 Y.-H. Chang, C.-W. Ku, Y.-H. Zhang, H.-C. Wang and J.-Y. Chen, Ultrafast Responsive Non-Volatile Flash Photomemory via Spatially Addressable Perovskite/Block Copolymer Composite Film, *Adv. Funct. Mater.*, 2020, **30**, 2000764, DOI: **10.1002/adfm.202000764**.

37 Z.-B. Liang, X. Chen, X.-J. Liao, J.-J. Li, Y. Yang, C.-F. Wang, Y.-X. Zheng and S. Chen, Continuous production of stable chiral perovskite nanocrystals in electrospinning nanofibers to exhibit circularly polarized luminescence, *J. Mater. Chem. C*, 2022, **10**, 12644–12651, DOI: **10.1039/D2TC02090D**.

38 J. Li, T. Cui, J. Yu, Z.-B. Liang, Y. Liang, J. Li and S. Chen, Stable and large-scale organic–inorganic halide perovskite nanocrystal/polymer nanofiber films prepared via a green in situ fiber spinning chemistry method, *Nanoscale*, 2022, **14**, 11998–12006, DOI: **10.1039/D2NR01691E**.

39 Y.-W. Harn, S. Liang, S. Liu, Y. Yan, Z. Wang, J. Jiang, J. Zhang, Q. Li, Y. He, Z. Li, L. Zhu, H.-P. Cheng and Z. Lin, Tailoring electrocatalytic activity of in situ crafted perovskite oxide nanocrystals via size and dopant control, *Proc. Natl. Acad. Sci. U. S. A.*, 2021, **118**, e2014086118, DOI: **10.1073/pnas.2014086118**.

40 S. Hou, Y. Guo, Y. Tang and Q. Quan, Synthesis and Stabilization of Colloidal Perovskite Nanocrystals by Multidentate Polymer Micelles, *ACS Appl. Mater. Interfaces*, 2017, **9**(22), 18417–18422, DOI: **10.1021/acsami.7b03445**.

41 K.-H. Wang, L.-C. Li, M. Shellaiah and K. Wen Sun, Structural and Photophysical Properties of Methylammonium Lead Tribromide ($MAPbBr_3$) Single Crystals, *Sci. Rep.*, 2017, **7**, 13643, DOI: **10.1038/s41598-017-13571-1**.

42 M. C. Brennan, C. L. McCleese, L. M. Loftus, J. Lipp, M. Febbraro, H. J. Hall, D. B. Turner, M. J. Carter, P. R. Stevenson and T. A. Grusenmeyer, Optically Transparent Lead Halide Perovskite Polycrystalline Ceramics, *ACS Appl. Mater. Interfaces*, 2024, **16**, 15084–15095, DOI: **10.1021/acsami.4c01517**.

43 D. Aldakov and P. Reiss, Safer-by-Design Fluorescent Nanocrystals: Metal Halide Perovskites vs Semiconductor Quantum Dots, *J. Phys. Chem. C*, 2019, **123**(20), 12527–12541, DOI: **10.1021/acs.jpcc.8b12228**.

44 N. Droseros, G. Longo, J. C. Brauer, M. Sessolo, H. J. Bolink and N. Banerji, Origin of the Enhanced Photoluminescence Quantum Yield in $MAPbBr_3$ Perovskite with Reduced Crystal Size, *ACS Energy Lett.*, 2018, **3**(6), 1458–1466, DOI: **10.1021/acsenergylett.8b00475**.

45 R. M. Silverstein, F. X. Webster and D. J. Kiemle, *Spectrometric Identification of Organic Compounds*, John Wiley & Sons, Inc., 7th edn, 2005, pp. 76–126, ISBN: 1118311655.

46 S. Lee, J. H. Park, B. R. Lee, E. D. Jung, J. C. Yu, D. D. Nuzzo, R. H. Friend and M. H. Song, Amine-Based Passivating Materials for Enhanced Optical Properties and Performance of Organic–Inorganic Perovskites in Light-Emitting Diodes, *J. Phys. Chem. Lett.*, 2017, **8**(8), 1784–1792, DOI: **10.1021/acs.jpclett.7b00372**.

47 J. Lee, Y. J. Choi, J. Yang, S. Ham, S. K. Jeon, J. Y. Lee, Y. Song, E. K. Ji, D. Yoon, S. Seo, H. Shin, G. S. Han, H. S. Jung, D. Kim and N. Park, *In situ* Formed Type I Nanocrystalline Perovskite Film for Highly Efficient Light-Emitting Diode, *ACS Nano*, 2017, **11**(3), 3311–3319, DOI: **10.1021/acsnano.7b00608**.

48 R. Wang, J. Xue, K. Wang, Z. Wang, Y. Luo, D. David Fenning, G. Xu, S. Nuryyeva, T. Huang, Y. Zhao, J. L. Yang, J. Zhu, M. Wang, S. Tan, I. Yavuz, K. N. Houk and Y. Yang, Constructive molecular configurations for surface-defect passivation of perovskite photovoltaics, *Science*, 2019, **366**, 1509–1513, DOI: **10.1126/science.aay9698**.

49 Y. Liu, K. Palotas, X. Yuan, T. Hou, H. Lin, Y. Li and S. Lee, Atomistic Origins of Surface Defects in $CH_3NH_3PbBr_3$ Perovskite and Their Electronic Structures, *ACS Nano*, 2017, **11**(2), 2060–2065, DOI: **10.1021/acsnano.6b08260**.

50 F. Wang, W. Geng, Y. Zhou, H.-H. Fang, C.-J. Tong, M. A. Loi, L.-M. Liu and N. Zhao, Phenylalkylamine Passivation of Organolead Halide Perovskites Enabling High-Efficiency and Air-Stable Photovoltaic Cells, *Adv. Mater.*, 2016, **28**, 9986–9992, DOI: **10.1002/adma.201603062**.

51 S. Singh, D. Mittal, V. Gurunarayanan, A. Sahu, R. Ramapanicker and V. G. Rao, Binding Strength-Guided Shuttling of Charge Carriers from Perovskite Nanocrystals to Molecular Acceptors, *ACS Appl. Energy Mater.*, 2023, **6**(15), 8091–8101, DOI: **10.1021/acsaem.3c01193**.

52 B. A. Koscher, J. K. Swabeck, N. D. Bronstein and A. P. Alivisatos, *J. Am. Chem. Soc.*, 2017, **139**(19), 6566–6569, DOI: **10.1021/jacs.7b02817**.

53 F. Haydous, J. M. Gardner and U. B. Cappel, The Impact of Ligands on the Synthesis and Application of Metal Halide Perovskite Nanocrystal, *J. Mater. Chem. A*, 2021, **9**, 23419–23443, DOI: **10.1039/D1TA05242J**.

54 S. Mann, *Biomineralization: Principles and Concepts in Bioinorganic Materials Chemistry*, Oxford Chemistry Masters, 2002, ISBN: 9780198508823.

55 M. D. Roy, S. K. Stanley, E. J. Amis and M. L. Becker, Identification of a Highly Specific Hydroxyapatite-binding Peptide using Phage Display, *Adv. Mater.*, 2008, **20**(10), 1830–1836, DOI: **10.1002/adma.200702322**.

56 J. Yu, M. L. Becker and G. A. Carri, A Molecular Dynamics Simulation of the Stability-Limited Growth Mechanism of Peptide-Mediated Gold-Nanoparticle Synthesis, *Small*, 2010, **6**, 2242–2245, DOI: **10.1002/smll.201000889**.

57 S. K. Stanley, M. L. Becker, E. K. Lin and W. Wu, Inhibitory Effects of a Phage-Derived Peptide on Au Nanocrystal Nucleation and Growth, *Langmuir*, 2009, **25**(18), 10886–10892, DOI: **10.1021/la901222k**.

58 M. A. Boles, D. Ling, T. Hyeon and D. V. Talapin, The surface science of nanocrystals, *Nat. Mater.*, 2016, **15**, 141–153, DOI: **10.1038/nmat4526**.

59 Y. Bai, M. Hao, S. Ding, P. Chen and L. Wang, Surface Chemistry Engineering of Perovskite Quantum Dots: Strategies, Applications, and Perspectives, *Adv. Mater.*, 2022, **34**, 2105958, DOI: **10.1002/adma.202105958**.

60 E. Holder, V. Marin, D. Kozodaev, M. A. R. Meier, B. G. G. Lohmeijer and U. S. Schubert, Iridium(III) Complexes with PEO and PS Polymer Macroligands and Light-Emitting Properties: Synthesis and Characterization, *Macromol. Chem. Phys.*, 2005, **206**, 989–997, DOI: **10.1002/macp.200400544**.

61 H. Cheng, Y. Feng, Y. Fu, Y. Zheng, Y. Shao and Y. Bai, Understanding and minimizing non-radiative recombination losses in perovskite light-emitting diodes, *J. Mater. Chem. C*, 2022, **10**, 13590–13610, DOI: **10.1039/D2TC01869A**.

62 A. Pfister and C. L. Fraser, Synthesis and Unexpected Reactivity of Iron Tris(bipyridine) Complexes with Poly (ethylene glycol) Macroligands, *Biomacromolecules*, 2006, **7**, 459–468, DOI: **10.1021/bm050652l**.

63 M. Chiper, R. Hoogenboom and U. S. Schubert, New terpyridine macroligands as potential synthons for supramolecular assemblies, *Eur. Polym. J.*, 2010, **46**, 260–269, DOI: **10.1016/j.eurpolymj.2009.10.021**.

64 F. M. Wisser, Y. Mohr, E. A. Quadrelli, D. Farrusseng and J. Canivet, Microporous Polymers as Macroligands for Pentamethylcyclopentadienylrhodium Transfer-Hydrogenation Catalysts, *ChemCatChem*, 2018, **10**, 1778–1782, DOI: **10.1002/cctc.201701836**.

65 J. Chiefari, Y. K. Chong, F. Ercole, J. Krstina, J. Jeffery, T. P. T. Le, R. T. A. Mayadunne, G. F. Meijs, C. L. Moad, G. Moad, E. Rizzardo and S. H. Thang, Living Free-Radical Polymerization by Reversible Addition–Fragmentation Chain Transfer: The RAFT Process, *Macromolecules*, 1998, **31**(16), 5559–5562, DOI: **10.1021/ma9804951**.